# Poly (styrene-*n*-butyl acrylate-methyl methacrylate)/Silica Nanocomposites Prepared by Emulsion Polymerization

**Qianping Rong, Aiping Zhu, Tao Zhong**

*College of Chemistry and Chemical Engineering, Yangzhou University, Yangzhou 225002, People's Republic of China*

Received 15 June 2010; accepted 7 October 2010
DOI 10.1002/app.33548
Published online 14 February 2011 in Wiley Online Library (wileyonlinelibrary.com).

**ABSTRACT:** Poly (styrene-*n*-butyl acrylate-methyl methacrylate) (PSBM)/silica nanocomposite was prepared by emulsion polymerization in the presence of oleic acid surface modified nanosilica. The structure, morphology, size, and size distribution were characterized by Fourier transform infrared (FTIR), transmission electron microscopy (TEM), and dynamics laser scattering. The chemical bond was formed between PSBM and nanosilica revealed by FTIR and TEM studies. The composite particles with an averaged diameter ranging from 30 to 80 nm have the core-shell structure. The effect of silica content on the glass transition temperature $T_g$, pyrolyze temperature, and rheological behavior of PSBM composites was systematically investigated. The results indicated that the addition of nanosilica could effectively inhibit chain movement, and improved the pyrolyze temperature of PSBM. The steady viscosity and dynamic modulus were strongly dependent on the content and distribution of nanosilica in PSBM nanocomposites. © 2011 Wiley Periodicals, Inc. J Appl Polym Sci 120: 3654–3661, 2011

**Key words:** nanosilica; PSBM nanocomposites; core-shell structure; rheological properties

## INTRODUCTION

During the past two decades, considerable efforts have been made to fabricate organic-inorganic nanocomposites, since they exhibit attractive mechanical,[1–5] thermal,[6,7] optical,[8] electrical,[9] and magnetic[10] properties. The organic–inorganic nanocomposites with well-defined structure and morphology are interesting and promising materials as their potential use in a wide range of conventional application fields.[11] Especially, silica-based organic–inorganic hybrid materials have been exploited applications in plastics, rubbers, coatings, and other industries.[12–14] Zhang et al.[15] prepared poly (methacrylic methacrylate) (PMMA)/silica hybrid materials via sol–gel process, which possessed high transparency and good heat-stability. Bokobza et al.[16] mixed silane coupling agent modified silica sols and acrylate monomers to obtain silica-based hybrid films after ultraviolet radiation. Chang et al.[17] prepared PMMA/silica nanocomposites via *in situ* polycondensation of alkoxysilane in the presence of trialkoxysilane-functionalized PMMA. Xia et al.[18] used the ultrasonic induced encapsulating emulsion polymerization technique to prepare polymer/inorganic nanocomposites.

On the other hand, the preparation of organic-inorganic nanohybrids through emulsion polymerization is more preferable because of its simple procedure. Percy et al.[19] reported the preparation of multicore type acrylic/silica nanocomposite particles in an emulsion with an averaged particle sizes of 110–220 nm, where the size of silica core was 13 or 22 nm. Ma et al. [20] reported recently the polyacrylate/silica nanocomposite prepared via sol–gel process by *in situ* emulsion polymerization. However, due to the large surface and strong aggregation of nanosilica, the synthesis of stable nanosilica/polymer composites through emulsion polymerization is difficult. The surface modification with a reactive coupling agent is an effective and versatile method to prevent the formation of agglomerated nanoparticles in emulsion polymerization.[21–23] After organically surface modification, the aggregation of nanosilica reduces greatly. In addition, good interfacial interactions are achieved between the inorganic core and the polymer shell. Therefore, emulsion polymerization has become a simple and effective technique to prepare polymer/silica nanocomposites with the inorganic core and polymeric shell structure. At the same time, hard nanosilica were well-dispersed into polymer matrix, which improved the strength,

*Correspondence to:* A. Zhu (apzhu@yzu.edu.cn).

Contract grant sponsor: China Jiangsu Provincial Natural and Scientific Grant; contract grant number: SBK200930208.

Contract grant sponsor: China Jiangsu Provincial Innovative Grant; contract grant number: SBC200910282.

Contract grant sponsor: Jiangsu Province, China; contract grant number: 08KJA430003.

**TABLE I**
**The Recipes for Preparing Silica-PSBM Nanocomposites Through Emulsion Polymerization**

| Components | Sil-0 | Sil-10 | Sil-20 |
|---|---|---|---|
| Styrene (g) | 4 | 4 | 4 |
| *n*-Butyl acrylate (g) | 3.5 | 3.5 | 3.5 |
| Methyl ethacrylate (g) | 2.5 | 2.5 | 2.5 |
| Modified silica (g) | / | 1 | 2 |
| Isopropanol (g) | / | 1 | 1 |
| APS (g) | 0.2 | 0.2 | 0.2 |
| SDS (g) | 0.6 | 0.6 | 0.6 |
| OP-10 (g) | 0.3 | 0.3 | 0.3 |
| $NaHCO_3$ (g) | 0.3 | 0.3 | 0.3 |
| Distilled water (g) | 88.6 | 85.6 | 85.6 |

adhesion, durability, and abrasion resistance of polymer materials.[24,25]

PSBM is widely to be used in preparing the coating. To improve the pyrolyze temperature of PSBM and the dispersion of nanosilica in PSBM, in this study, PSBM/silica nanocomposite was prepared by emulsion polymerization in the presence of oleic acid surface modified nanosilica. Our results demonstrated the core-shell structure of PSBM/silica composites and the chemical bond formed between PSBM and nanosilica. The good dispersibility of nanosilica in PSBM composites and the excellent interfacial adhesion resulted in the improvement of thermal decomposition and rheological behaviors of PSBM nanocomposites.

## MATERIALS AND METHODS

### Materials

Fumed silica ($SiO_2$) nanoparticles with an average diameter of 25 nm were supplied by Shanghai Chemical, China. The nanoparticles were dried at 120°C under vacuum for 24 h to eliminate the physically absorbed and weakly chemically adsorbed species. Oleic acid was purchased by Shanghai Chemical Reagent, China. Technical-grade monomers *n*-butyl acrylate (BA), styrene (St), methyl methacrylate (MMA) with 10–20 ppm of hydroquinone monomethyl ether (MEHQ) were purchased from Guangzhou Langri Chemical, China. The monomers were purified by distillation before use. The emulsifiers (nonyl phenol polyoxyethylene ether (OP-10) and sodium dodecyl sulfate (SDS), sodium bicarbonate ($NaHCO_3$), and ammonium persulfate (APS) were used as received. The organic solvents, such as ethanol, isopropanol, and toluene, were analytical reagent. Doubly deionized water (DDI water) was used throughout the study.

### Modification of nanosilica by oleic acid

Fumed silica (6.3 g) was first dispersed into 90 mL distillated water with the aid of ultrasonic for 3 h. 1.5 mL oleic acid was added into the dispersion and vigorously stirred for 90 min at room temperature using a magnetic stirrer. Then, 5 mL of 25 wt % aqueous ammonia solution was charged into the solution and agitated overnight. The dispersion was neutralized with 30 wt % aqueous HCl solution. The mixture was centrifuged (2500 rpm) for 30 min, and the obtained precipitates were washed three times with 15 mL 1/1 ethanol/water (V/V) mixed solvent to remove excess amount of oleic acid. The cleaned precipitates were dried in oven under vacuum at 50°C for 24 h.

### Preparation of core-shell PSBM nanocomposites

St, BA, and MMA monomers with a weight ratio of 8 : 7 : 5 were polymerized in the presence of oleic acid surface modified nanosilica by semibatch emulsion polymerization. The reaction was carried out in a 250-mL four-necked round bottomed glass reactor, which was equipped with a reflux condenser, a mechanical stirrer, a dropping funnel, and a nitrogen gas inlet. The details of the reaction recipe were described in Table I. In a typical synthesis, 1 g modified nanosilica was dispersed in the aqueous solution, in which 1 g of isopropanol, 0.6 g SDS, 0.3 g of OP-10, 0.3 g $NaHCO_3$, and 80 mL of DDI-water were added and ultrasonically treated for 2 h. Styrene (4 g), *n*-butyl acrylate (3.5 g), and methyl methacrylate (2.5 g) were premixed and poured into the dropping funnel. The initiator (APS) was dissolved in a definite amount of DDI water. The nanosilica suspension was transferred to the reactor vessel. When the reaction system was heated to 75°C, both the monomer mixture and initiator solution were added to the reactor dropwisely at the same time. After 4 h of feeding, the reaction system was heated to 90°C for another 1 h. After that, the polymerization system was cooled to room temperature. For comparison purpose, the PSBM latex without presence of nanosilica was prepared by conventional emulsion polymerization using the same monomer weight ratio (St : BA : MMA, 8 : 7 : 5). The PSBM latex and the PSBM nanocomposites with 10 wt % and 20 wt % of nanosilica was designated as Sil-0, Sil-10, and Sil-20.

To obtain PSBM composite particles, the saturated NaCl solution was added to the composite latex and the composite particles precipitated from the suspension. The precipitate was washed with DDI water for three times and dried at 45°C under vacuum. A transparent film was obtained when the composite latex was cast in a poly(tetrafluoroethylene) (PTFE) dish and slowly dried in a controlled atmosphere at 50°C.

### Characterization

FTIR was applied to characterize the chemical structures of PSBM nanocomposites. A (TE CHAI-12)

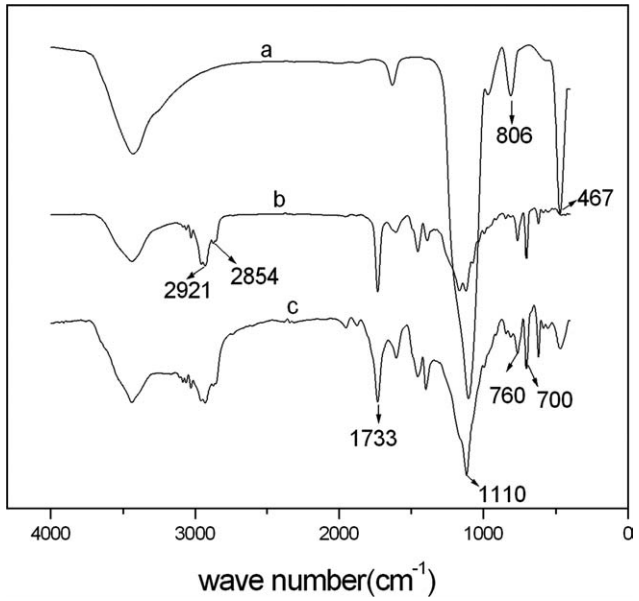


**Figure 1** The FTIR spectra of (a) nanosilica, (b) Sil-0, and (c) Sil-10.

(Philips) transmission electron microscope (TEM) was used to observe the morphologies of PSBM nanocomposites. The sample lattices were diluted and ultrasonic treated at 25°C for 15 min and dried on carbon coated copper grids. TGA measurements were performed on a NETZSCH STA 409PC thermogravimetric analyzer from 25 to 800°C at a heating rate of 10°C/min under the flow of anhydrous air. The PSBM content grafted on the nanosilica was subsequently measured. The glass transition temperatures of composite films were determined by differential scanning calorimetry (DSC). To eliminate water influence (crystal water), two runs were scanned, from −20 to 100°C, held at this temperature for 10–15 min and run again from –20 to 100°C at a heating rate of 10°C/min under $N_2$ flow. The results of the second cycle were used to determine $T_g$. The hydrodynamic radius and size distribution were determined by DLS using a Brookhaven BI9000AT light scattering system (Brookhaven Instruments Corp., USA). All the DLS measurements were repeated three times with an incident wavelength of 658 nm. Before measurement, composite lattices were diluted with distilled water to 0.1% (wt) concentration. The measurement was triplicated, and the final results were the average of three runs. To observe the morphology of interfacial adhesion of PSBM composites, the PSBM composite specimen was fractured after immersed into the liquid nitrogen. The fractured section surfaces were coated with a thin layer (10–20 nm) of gold–palladium before FESEM examination. Rheological measurements were carried out on a rheometer (HAAKE RS600 rheometer, Thermo Electron, USA) equipped with a parallel plate geometry using 20 mm diameter plates. All measurements were performed with a 200 FRTN1 transducer with a lower resolution limit of 0.02 g cm. In a steady shear measurement, the stress and viscosity response to the shear rates (0.0001–10 $s^{-1}$) were recorded at the temperature of 180°C. In a viscoelastic measurement, the dynamic strain sweep measurement was carried out first to determine the linear viscoelastic region. Then, a dynamic frequency sweep measurement was carried out at the strain of 1%.

## RESULTS AND DISCUSSION

### Characterization of PSBM/silica nanocomposites

#### FTIR analysis

Ding et al.[26] first applied oleic acid as a functionalized monomer and found oleic acid could adhere to silica surface by a single hydrogen bonding. In this study, oleic acid was chosen as the surface modification agent to prepare a stable emulsion polymerization system in the presence of nanosilica. However, it is inevitable to produce a certain amount of latex particles not containing the nanosilica. To remove the free PSBM, PSBM composite lattices were extracted with acetone for 24 h. Figure 1 showed the FTIR spectra of silica, Sil-0 and purified Sil-10. In the spectrum of nanosilica [Fig. 1(a)], a pronounced band at 1108 $cm^{-1}$ together with two less pronounced bands at 806 and 467 $cm^{-1}$ appeared, which is corresponding to the vibration absorption of Si—O—Si. In the spectrum of Sil-0 [Fig. 1(b)], the peaks at 2921, 2854, 1733, 760, and 700 $cm^{-1}$ were associated with the characteristic vibration of methyl ($CH_3$), methylene ($CH_2$), carbonyl (C=O), and benzyl groups. In the spectrum of Sil-10 [Fig. 1(c)], compared with that of PSBM, the peaks at 1110 and 467 $cm^{-1}$ appeared, which were the characteristic peaks of Si—O—Si. Such results indicated that there are chemical bonds formed between PSBM and nanosilicas.

#### TEM

To elucidate the formation of core-shell morphology of PSBM/surface-modified nanosilica, the composite particles were dispersed in toluene (a good solvent for PSBM, because pure PSBM can be completely dissolved in toluene) overnight under stirring. If there was not chemical bond between nanosilica and PSBM, nanosilicas would be separated. The TEM image of extracted composite particles (Sil-10) was shown in Figure 2. It demonstrated the bright spherical cores with an average diameter of 25 nm, which should be nanosilicas, and the dark color surrounding the nanosilica core should be the

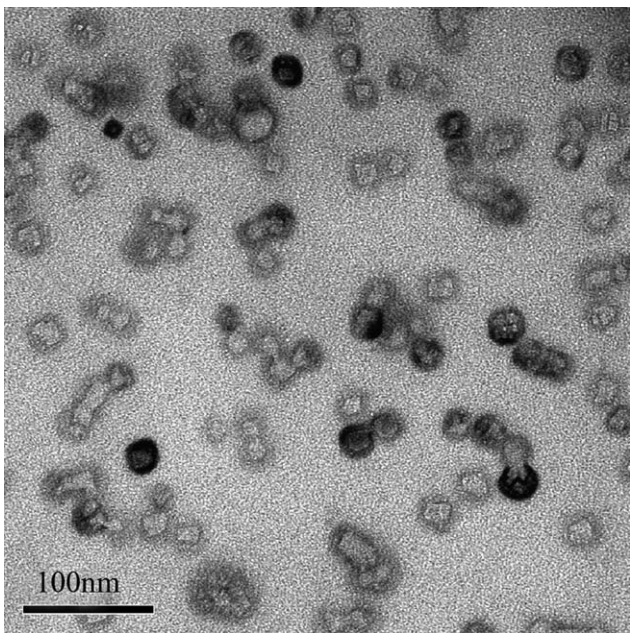


**Figure 2** TEM images of Sil-10, before measurement the sample was dispersed in toluene (a good solvent for PSBM).

grafted PSBM shell. Moreover, most of nanoparticles showed well-dispersed appearance. The results reinforced the formation of chemical bonds between nanosilica and PSBM, and nanosilica has been effectively encapsulated by PSBM.

Figure 3 showed the TEM morphologies of nanosilica and PSBM composites. Figure 3(a) revealed the averaged diameter of 25 nm for nanosilica and the strong interparticle aggregation. Figure 3(b,c) showed the morphologies of Sil-10 and Sil-20 composites. The diameters of Sil-10 and Sil-20 composite particles were 30 ± 7.5 nm and 50 ± 25.0 nm. Both PSBM composite particles appeared well-dispersed regular spherical morphology. Figure 3(d) presented the magnification image of Figure 3(c), which suggested the core-shell structure for the PSBM/silica nanocomposites prepared via emulsion polymerization in the presence of the oleic acid surface-modified nanosilica.

Figure 4 compared the FESEM fractographs of Sil-10 and Sil-20. From Figure 4(a,c), rough and adhesive interfaces were found. From Figure 4(b,d), the composite particles with a diameter around 50 nm were observed. At higher nanosilica content, the interface between inorganic and polymeric phases became more compatible [Fig. 4 (d)] comparing with Sil-10 [Fig. 4 (c)]. However, the FESEM fractographs of Sil-0 [Fig. 4 (e)] demonstrates smooth morphology in comparison with that of PSBM composite. The

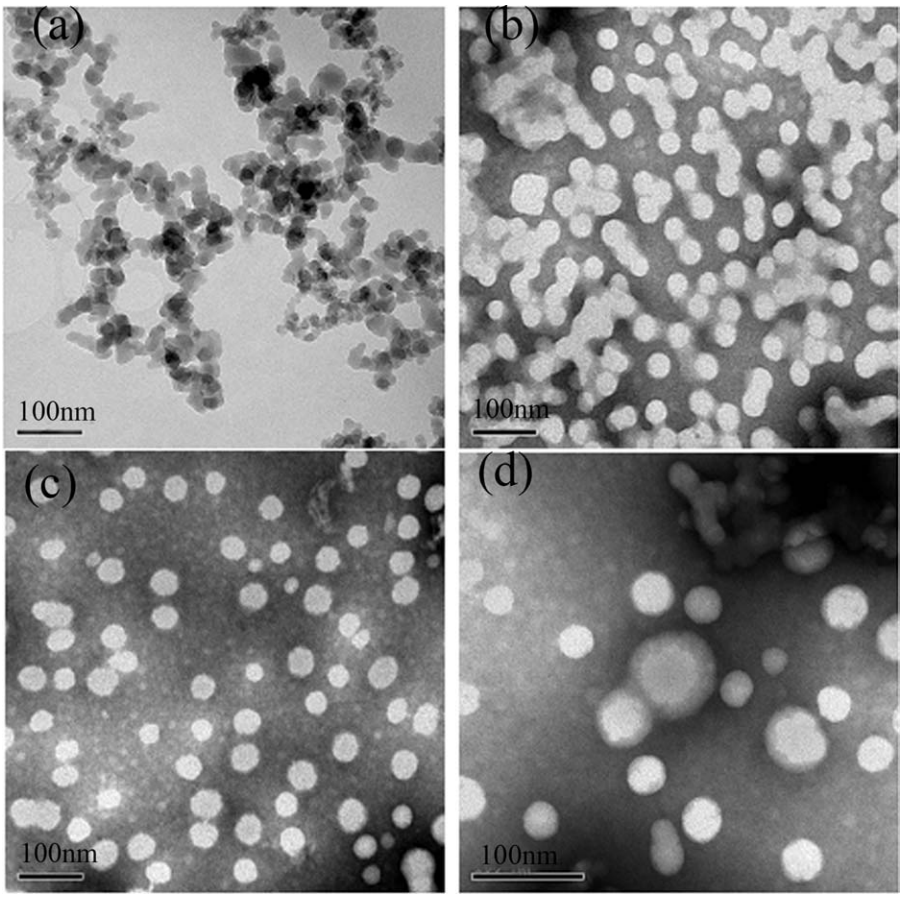


**Figure 3** TEM of nanosilica and PSBM nanocomposites (a) nanosilica, (b) Sil-10, (c) Sil-20, and (d) Sil-20 at higher magnification.

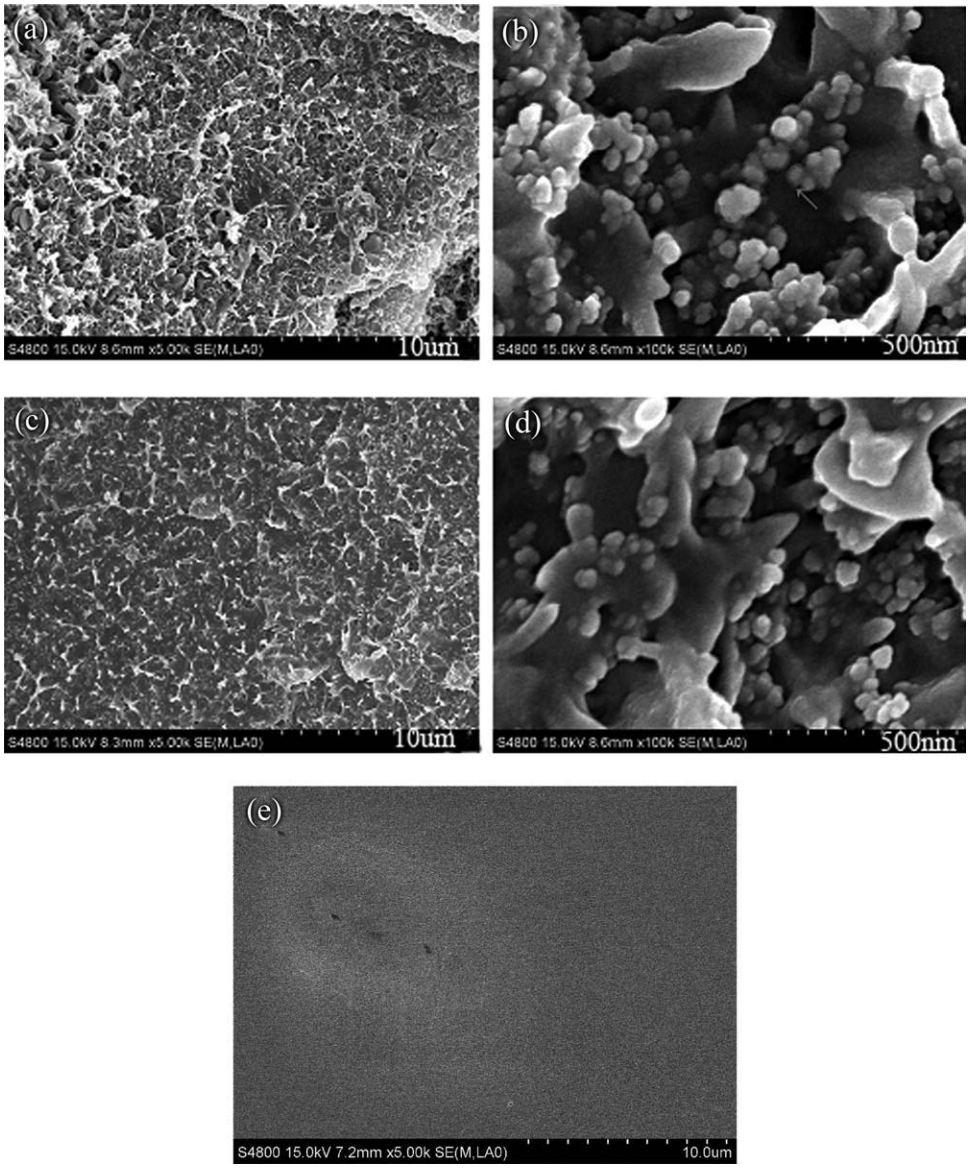


**Figure 4** FESEM images for (a) Sil-10, (b) magnification of (a), (c) Sil-20, (d) magnification of (c), and (e) Sil-0.

enhanced dispersion of nanosilica in PSBM matrix was caused by the core-shell structure of nanocomposites. It was well known that the more dispersed the nanosilica was, the better the interface between nanosilica and polymer matrix achieved. The surface hydroxyl groups of unmodified nanosilica had an tendency to form agglomerates. Moreover, hydrophobic PSBM polymers were not able to wet and interact with hydrophilic fillers.[23] In the case of polymer-encapsulated nanosilica composites, the dispersion of nanosilica was improved substantially [Fig. 4(b,d)] due to the steric hindrance caused by polymer long chain encapsulation. In addition, the chemical bond between polymer shell and nanosilica core led to the interfacial compatibility enhancement between inorganic and polymeric phases. The FESEM morphology clearly demonstrated polymer shell/nanosilica core structure favored the interfacial improvement of polymer/silica nanocomposites.

## DLS

The particle radius distributions of PSBM and its composite lattices were shown in Figure 5. The radius distribution of the PSBM composite lattices appeared two peaks. The small and big particles for Sil-10 were 19 $\pm$ 3.5 nm and 98 $\pm$ 25.0 nm in radius, and the small and big particles for Sil-20 were 21 $\pm$ 5.5 nm and 138 $\pm$ 28.0 nm in radius. Comparing the size of nanosilica of 25 nm and the pure PSBM (Sil-0), we can conclude that the small particle in composite latex should be related to the free PSBM latex and the big one should be attributed to the core-shell PSBM/nanosolica composite particles.

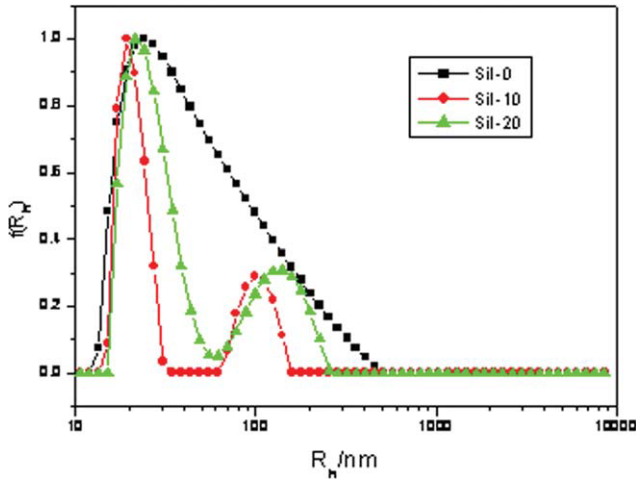


**Figure 5** DLS particle radius distribution of (a) Si-0 and (b) Sil-10 and Sil-20 latex. [Color figure can be viewed in the online issue, which is available at wileyonlinelibrary.com.]

## Thermal analysis

### DSC

Figure 6 compared the DSC traces of dried PSBM and cleaned PSBM/silica nanocomposites. The glass transition temperatures ($T_g$) for Sil-0, Sil-10, and Sil-20 were found to be 37.8, 35.3, and 34.7°C. There was a little decrease of $T_g$, this decrease may be caused by the low molecular oleic acid on the nanosilicas. Moreover, the vitrification transforms became less obvious for the PSBM composites.

### TGA and DTA

Figure 7 showed the curves of TGA and DTA of Sil-0, Sil-10, and Sil-20. In the TGA thermograms, the weight loss between 190 and 400°C corresponded to the thermal oxidation and pyrolysis of polymer. The

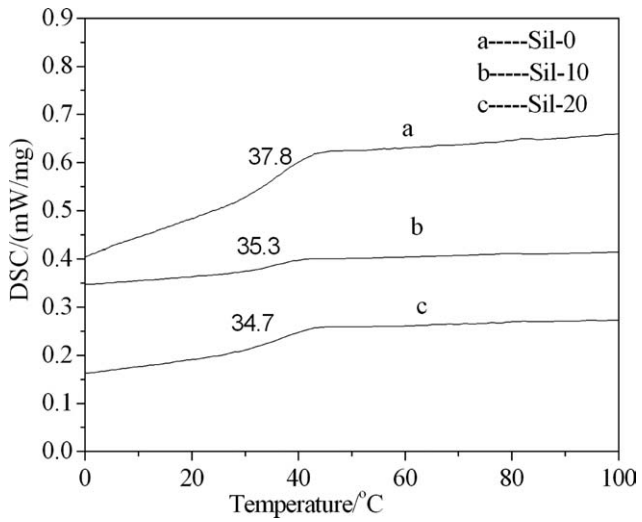


**Figure 6** DSC thermograms of dried Sil-0, Sil-10, and Sil-20.

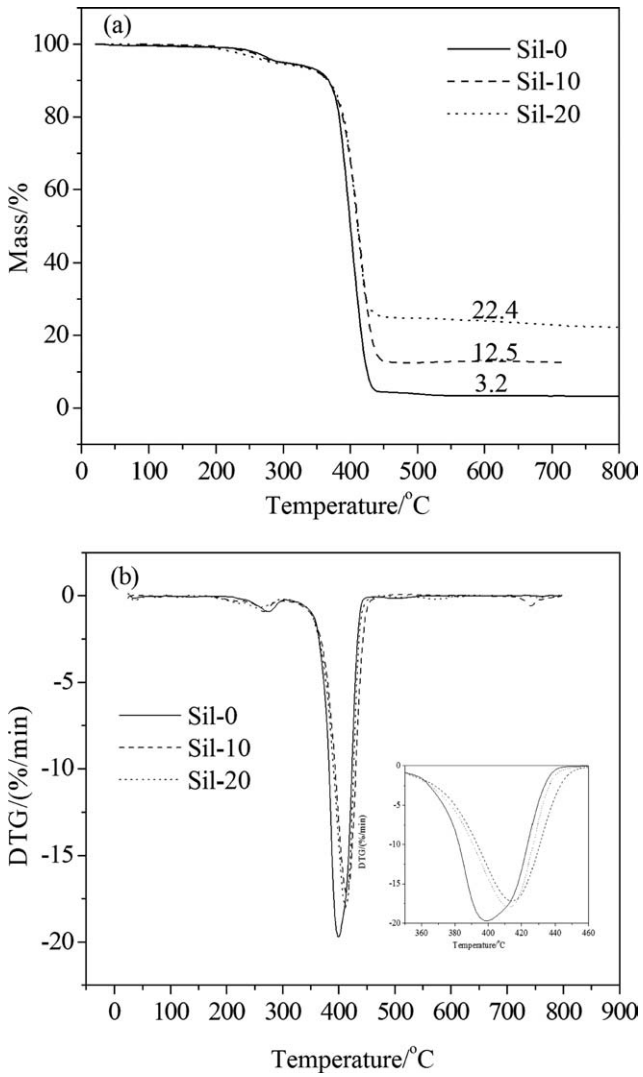


**Figure 7** TGA and DTA curves of dried Sil-0, Sil-10, and Sil-20. (a) TGA, (b) DTA.

nanosilica content in the nanocomposites could be estimated by the balance value of TGA, which was found to be 3.2, 12.5, and 22.4 wt % for Sil-0, Sil-10, and Sil-20. The TGA results were consistent with the initial design (10 and 20 wt % of nanosilica for Sil-10 and Sil-20 composites). From the DTA curve of Sil-0, Sil-10, and Sil-20, the pyrolytic temperatures were determined to be 400.5, 413.5, and 412.0°C for Sil-0, Sil-10, and Sil-20. The shift on the pyrolytic temperature of nanocomposites comparing with that of Sil-0 indicated the thermal stability of PSBM nanocomposite had been improved after introducing nanosilica.

## Rheological properties

### Steady-state flow properties

The variation of steady state viscosity ($\eta$) as a function of shear rate ($\dot{\gamma}$) was presented in Figure 8. All nanocomposite melts exhibited pseudoplastic

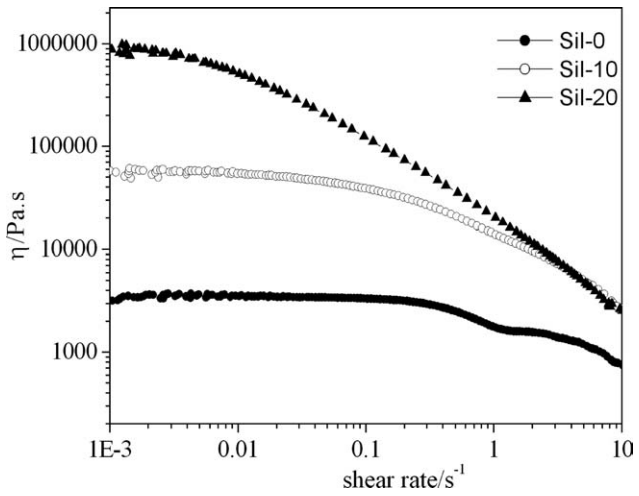


**Figure 8** The viscosity (η) of dried Sil-0, Sil-10, and Sil-20 from steady-shear sweep at the temperature of 180°C.

behavior within experimental shear rate range. The low shear viscosity of Sil-0 was lower than those of nanocomposites, and the low shear viscosity of Sil-20 was 10 times of Sil-10. The results suggested the chemically bonded nanosilica in PSBM composites perturbed the normal flow and hindered the mobility of chain segments,[27] which leading to the increase in viscosity with increasing nanosilica content.

## Dynamic rheological properties

The dynamic strain sweep was conducted to determine linear viscoelastic region. Figure 9 showed the dependence of dynamic moduli on strain (γ) for Sil-0, Sil-10, and Sil-20. The linear viscoelastic region decreased with increasing nanosilica. After the critical strain values, the curves started to drop down. Therefore, the following dynamic frequency oscillatory measurements were conducted at $\gamma \sim 1\%$.

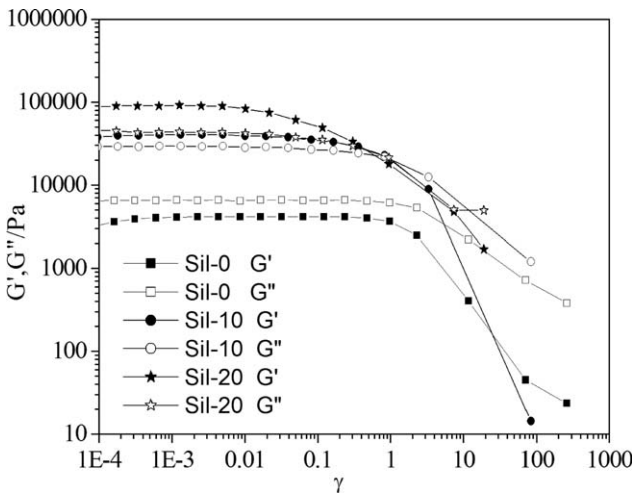


**Figure 9** The $G'$ and $G''$ of dried Sil-0, Sil-10, and Sil-20 in dynamic strain sweep at the temperature of 180°C.

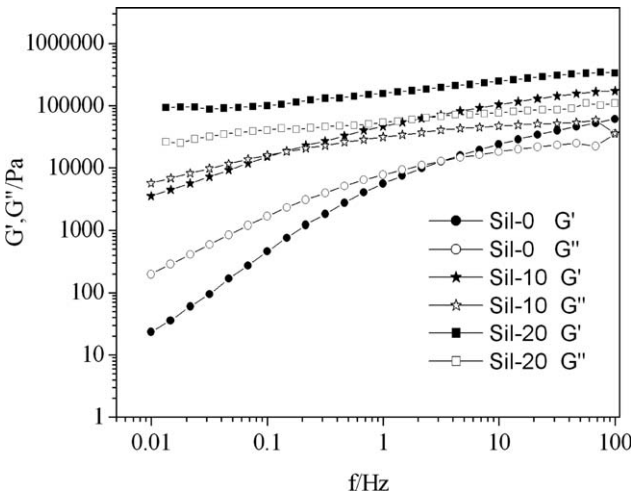


**Figure 10** Frequency dependence of the storage modulus ($G'$, filled symbol) and loss modulus ($G''$, open symbol) at the temperature of 180°C and strain of 1%.

The frequency dependence of storage modulus ($G'$) and loss modulus ($G''$) for Sil-0, Sil-10, and Sil-20 were showed in Figure 10. Both moduli ($G'$ and $G''$) increased with nanosilica contents. For the samples of Sil-0 and Sil-10, $G''$ was higher than $G'$ at low frequency ranges and the $G''$ became higher than $G'$ at high frequency ranges, which indicated flow properties and elastic properties dominated at small and large frequency ranges, respectively. The decrease in the crossover frequency while increasing nanosilica load, which suggested that the relaxation time increased and the segmental motion decreased. From rheological investigation, it was clear that nanoparticles played an important role in inhibiting polymer segmental motion. According to Tsagaropoulos and Eisenberg,[28] the interaction of polymer chains with nanosized silica particles reduced the mobility of polymer chains and led to the formation of immobilized and restricted mobility regions around the nanosilica particles. The $G'$ was always higher than $G''$ in the experimental frequency range for Sil-20, which indicated the elastic strength of Sil-20 was significantly improved. Also, the plateaus of $G'$ and $G''$ for Sil-20 in the range of low frequencies indicated that a network formed from silica nanoparticles.

## CONCLUSIONS

PSBM/silica nanocomposites were successfully prepared by semibatch emulsion polymerization in the presence of oleic acid surface-modified nanosilica. The composite nanoparticles demonstrated core-shell nanostructures with a diameter ranging from 20 to 80 nm. The glass transition temperature was little dependent on the nanosilica content of nanocomposites and the pyrolyze temperature improved 16°C after nanosilica introduction. The interfacial

morphology indicated the excellent interfacial adhesion between nanosilica and PSBM due to the formation chemical bonding formed between PSBM and nanosilica, which resulted in the improvement rheologic hardness of PSBM nanocomposites.

## References


1. Frohlich, J.; Niedermeier, W.; Luginsland, H. D. Compos Part A: Appl Sci Manufact 2005, 36, 449.
2. Bandyopadhyay, A.; De Sarkar, M.; Bhowmick, A. K. J Appl Polym Sci 2005, 95, 1418.
3. Odegard, G. M.; Clancy, T. C.; Gates, T. S. Polymer 2005, 46, 553.
4. Ragosta, G.; Abbate, M.; Musto, P.; Scarinzi, G.; Mascia, L. Polymer 2005, 46, 10506.
5. Mizutani, T.; Arai, K.; Miyamoto, M.; Kimura, Y. Progr Org Coat 2006, 55, 276.
6. Zheng, K.; Chen, L.; Li, Y.; Cui, P. Polym Eng Sci 2004, 44, 1077.
7. Chiang C. L.; Ma, C. M. Polym Degrad Stab 2004, 83, 207.
8. Wang, Y. W.; Yen, C. T.; Chen, W. C. Polymer 2005, 46, 6959.
9. Wang, Y.; Wang, X.; Li, J.; Mo, Z.; Zhao, X.; Jing, X.; Wang, F. Adv Mater 2001, 13, 1582.
10. Salgueirino-Maceira, V.; Correa-Duarte, M. A.; Spasova, M.; Liz-Marzan, M.; Farle, M. Adv Funct Mater 2006, 16, 509.
11. Castelvetro, V.; De Vita, C. Adv Colloid Interface Sci 2004, 108-109, 167.
12. Kashiwagi, T.; Morgan, A. B.; Antonucci, J. M.; VanLandingham, M. R.; Harris, R. H., Jr; Awad, W. H.; Shields, J. R. J Appl Polym Sci 2003, 2072, 89.
13. Peng, Z.; Kong, L. X.; Li, S. D.; Chen, Y.; Huang, M. F. Compos Sci Technol 2007, 67, 3130.
14. Mammeri, F.; Rozes, L.; Le Bourhis, E.; Sanchez, C. J Eur Ceramic Soc 2006, 26, 267.
15. Zhang, Q. W.; Zhang, Y. H.; Chen, S. M. Appli Chem 2002, 9, 874.
16. Bokobza, L.; Garnaud, G.; Mark, J. E.; Jethmalani, J. M.; Seabolt, E. E.; Ford, W. T. Chem Mater 2002, 14, 162.
17. Chang, T. C.; Wang, Y. T.; Hong, Y. S.; Chiu, Y. S. J Polym Sci Part A: Polym Chem 2000, 1972, 38.
18. Xia, H.; Zhang, C.; Wang, Q. J Appl Polym Sci 2001, 80, 1130.
19. Percy, M. J.; Amalvy, J. I.; Randall, D. P.; Armes, S. P.; Greaves, S. J.; Watts, J. F. Langmuir 2004, 20, 2184.
20. Ma, J. Z.; Hu, J.; Zhang, Z. J. Eur Polym J 2007, 43, 4169.
21. Amdouni, N.; Sautereau, H.; Gerard, J. F. J Appl Polym Sci 1992, 46, 1723.
22. Reculusa, S.; Mingotaud, C.; Bourgeat-Lami, E.; Duguet, E.; Ravaine, S. Nano Lett 2004, 4, 1677.
23. Ruckenstein, E.; Park, J. S. Polymer 1992, 33, 405.
24. Alexandre, M.; Dubois, P. Mater Sci Eng: R: Reports 2000, 28, 1.
25. Giannelis, E. P.; Krishnamoorti, R.; Manias, E. Adv Polym Sci 1999, 138, 107.
26. Ding, X.; Zhao, J.; Liu, Y.; Zhang, H.; Wang, Z. Mater Lett 2004, 58, 3126.
27. Tang, E.; Cheng, G.; Shang, Q.; Ma, X. Progr Org Coatings 2006, 57, 282.
28. Tsagaropoulos, G.; Eisenberg, A. Macromolecules 1995, 28, 6067.